

Planck 2015

Part 1: An Overview

Jayanti Prasad
IUCAA/CMS (Pune University), Pune

October 12, 2015

Planck Summarized

- Launched on 14 May 2009, made observations between 12 August 2009 and 23 October 2013; Nominal Mission : 15.5 months (2013 release), Full mission : 29 Months, 4.8 Surveys (2015 release)
- The mission was designed to study the Cosmic Microwave Background (CMB), the relic radiation from the Big Bang, **with an accuracy defined by fundamental astrophysical limits.**
- 74 detectors covering nine frequency bands :
 - LFI : 30, 44, 70 Ghz
 - HFI : 100, 143, 217, 353, 545, 857 GHz.
- Resolution : 33'-5'
- Planck imaged the whole sky twice in one year, with a combination of sensitivity, angular resolution, and frequency coverage never before achieved.

Some progress since Planck 2013

- The dip at $l = 1800$ due 4K cooler line at 217 Ghz has been resolved.
- There was 2.6 % calibration offset between WMAP9 and Planck which has been resolved.
- Beam has been characterized more accurately as compared to 2013, many new low level data processing improvements.
- Planck 2013 used low-l polarization from WMAP 9 (for constraining τ) which is not the case for 2015.
- Now high-l likelihood is computed with “Plik” and not “CamSpec”.

CMB and foregrounds

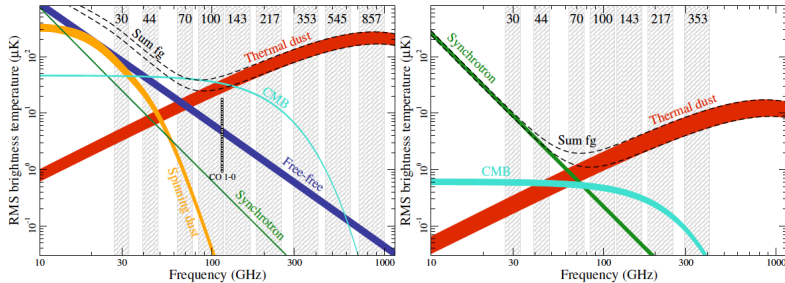


Fig. 16. Brightness temperature rms as a function of frequency and astrophysical component for temperature (left) and polarization (right). For temperature, each component is smoothed to an angular resolution of 1° FWHM, and the lower and upper edges of each line are defined by masks covering 81 and 93 % of the sky, respectively. For polarization, the corresponding smoothing scale is 40', and the sky fractions are 73 and 93 %.

The Telescope

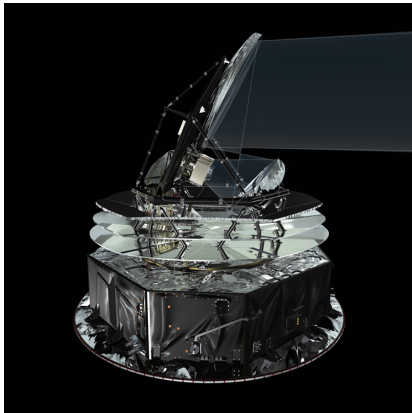


Figure : Planck Telescope

Artist's impression of radiation being collected and focused by the telescope's primary and secondary mirrors. The radiation is then directed to the focal planes of LFI & HFI which convert the lower energy microwaves into electrical voltages (like a transistor radio) and converts higher energy microwaves to heat and is measured by a tiny electrical thermometer.

Planck's Orbit

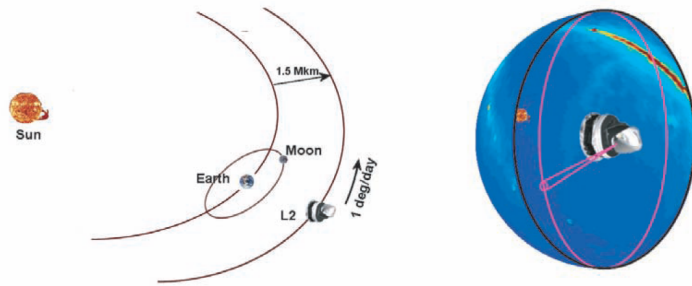
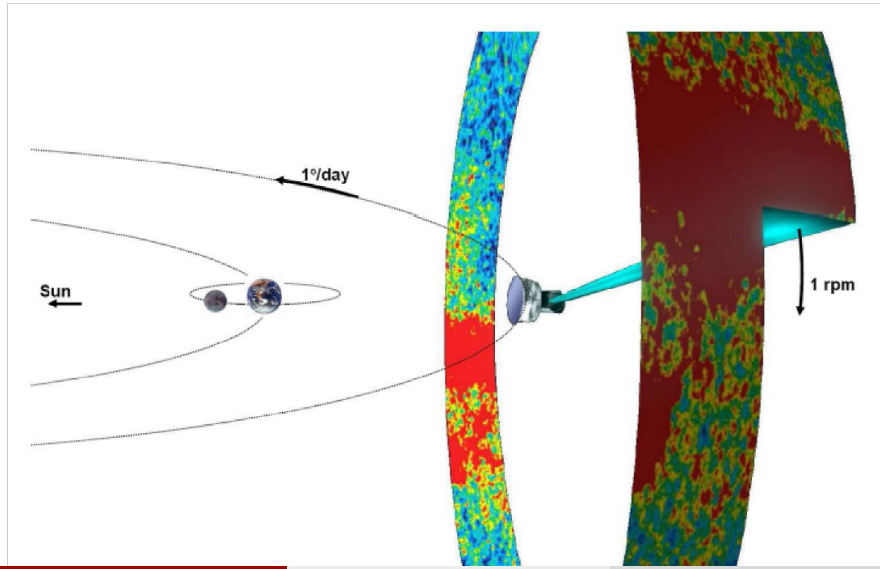


FIG 1.4.—Planck orbit at the 2nd Lagrangian point of the Earth-Sun system (L_2). The spin axis is pointed near the Sun, with the solar panel shading the payload, and the telescope sweeps the sky in large circles at 1 rpm.

Planck's Orbit



Specs of LFI

Table 5. Main characteristics of LFI full mission maps.

| Characteristic | Frequency band | | |
|---|----------------|--------|--------|
| | 30 GHz | 44 GHz | 70 GHz |
| Centre frequency [GHz] | 28.4 | 44.1 | 70.4 |
| Effective beam FWHM ^a [arcmin] | 32.29 | 27.00 | 13.21 |
| Effective beam ellipticity ^a | 1.32 | 1.04 | 1.22 |
| Temperature noise (1°) ^b [μK_{CMB}] | 2.5 | 2.7 | 3.5 |
| Polarization noise (1°) ^b [μK_{CMB}] | 3.5 | 4.0 | 5.0 |
| Overall calibration uncertainty ^c [%] | 0.35 | 0.26 | 0.20 |
| Systematic effects uncertainty in Stokes I^d [μK_{CMB}] | 0.19 | 0.39 | 0.40 |
| Systematic effects uncertainty in Stokes Q^d [μK_{CMB}] | 0.20 | 0.23 | 0.45 |
| Systematic effects uncertainty in Stokes U^d [μK_{CMB}] | 0.40 | 0.45 | 0.44 |

^a Calculated from the main beam solid angle of the effective beam, $\Omega_{\text{eff}} = \text{mean}(\Omega)$. These values are used in the source extraction pipeline (Planck Collaboration XXVI 2015).

^b Noise rms computed after smoothing to 1° .

^c Sum of the error determined from the absolute and relative calibration, see Planck Collaboration IV (2015).

^d Estimated rms values over the full sky and after full mission integration. Not included here are gain reconstruction uncertainties, estimated to be of order 0.1 %.

Specs of HFI

Table 6. Main characteristics of HFI full mission maps.

| Characteristic | Reference frequency ν [GHz] | | | | | | Notes |
|---|---------------------------------|--------|-------|-------|---------|---------|-------|
| | 100 | 143 | 217 | 353 | 545 | 857 | |
| Number of bolometers | 8 | 11 | 12 | 12 | 3 | 4 | a1 |
| Effective beam FWHM ₁ [arcmin] | 9.68 | 7.30 | 5.02 | 4.94 | 4.83 | 4.64 | b1 |
| Effective beam FWHM ₂ [arcmin] | 9.66 | 7.22 | 4.90 | 4.92 | 4.67 | 4.22 | b2 |
| Effective beam ellipticity ϵ | 1.186 | 1.040 | 1.169 | 1.166 | 1.137 | 1.336 | b3 |
| Noise per beam solid angle [μK_{CMB}] | 7.5 | 4.3 | 8.7 | 29.7 | | | c1 |
| [kJy sr^{-1}] | ... | ... | ... | ... | 9.1 | 8.8 | c1 |
| Temperature noise [μK_{CMB} deg] | 1.29 | 0.55 | 0.78 | 2.56 | ... | ... | c2 |
| [kJy sr^{-1} deg] | ... | ... | ... | ... | 0.78 | 0.72 | c2 |
| Polarization noise [μK_{CMB} deg] | 1.96 | 1.17 | 1.75 | 7.31 | ... | ... | c3 |
| Calibration accuracy [%] | 0.09 | 0.07 | 0.16 | 0.78 | 1.1(+5) | 1.4(+5) | d |
| CIB monopole prediction [MJy sr^{-1}] | 0.0030 | 0.0079 | 0.033 | 0.13 | 0.35 | 0.64 | e |

^{a1} Number of bolometers whose data were used in producing the channel map.

^{b1} FWHM of the Gaussian whose solid angle is equivalent to that of the effective beams.

^{b2} FWHM of the elliptical Gaussian fit.

^{b3} Ratio of the major to minor axis of the best-fit Gaussian averaged over the full sky.

^{c1} Estimate of the noise per beam solid angle, as given in *b1*.

^{c2} Estimate of the noise in intensity scaled to 1° assuming that the noise is white.

^{c3} Estimate of the noise in polarization scaled to 1° assuming that the noise is white.

^d Calibration accuracy (at 545 and 857 GHz, the 5 % accounts for the model uncertainty).

^e According to the [Béthermin et al. \(2012\)](#) model, whose uncertainty is estimated to be at the 20 % level (also for constant νI_ν).

Planck 2015 : Publications

- I. Overview of products and results (*this paper*)
- II. Low Frequency Instrument data processing
 - III. LFI systematic uncertainties
 - IV. LFI beams and window functions
 - V. LFI calibration
 - VI. LFI maps
- VII. High Frequency Instrument data processing: Time-ordered information and beam processing
- VIII. High Frequency Instrument data processing: Calibration and maps
- IX. Diffuse component separation: CMB maps
- X. Diffuse component separation: Foreground maps
- XI. CMB power spectra, likelihood, and consistency of cosmological parameters
- XII. Simulations
- XIII. Cosmological parameters
- XIV. Dark energy and modified gravity
- XV. Gravitational lensing
- XVI. Isotropy and statistics of the CMB
- XVII. Primordial non-Gaussianity
- XVIII. Background geometry and topology of the Universe
- XIX. Constraints on primordial magnetic fields
- XX. Constraints on inflation
- XXI. The integrated Sachs-Wolfe effect
- XXII. A map of the thermal Sunyaev-Zeldovich effect
- XXIII. The thermal Sunyaev-Zeldovich effect–cosmic infrared background correlation
- XXIV. Cosmology from Sunyaev-Zeldovich cluster counts
- XXV. Diffuse, low-frequency Galactic foregrounds
- XXVI. The Second Planck Catalogue of Compact Sources
- XXVII. The Second Planck Catalogue of Sunyaev-Zeldovich Sources
- XXVIII. The Planck Catalogue of Galactic Cold Clumps

Plan of the program

| S. No | Speaker | Topics | Date |
|-------|-------------------|--|--------------------------|
| 1 | Jayanti Prasad | Overview Power spectra & Likelihoods Cosmological Parameters | October, 12: 15:30-17.00 |
| 2 | Pavan K. Aluri | Isotropy & Statistics | Oct 19, 14:30-17.00 |
| 3 | Suvodip Mukherjee | Integrated Sachs-Wolfe Effect Constraints on Inflation Joining BICEP-KECK-Planck (BKP) | |
| 4 | Shabir Shekh | Gravitational Lensing Gravitational Lensing -IR corr | |

Data Products

-
- Maps of the cosmic microwave background (CMB) at nine frequencies in temperature, and at seven frequencies (30 - 353 GHz) in polarization.
- Maps of the thermal Sunyaev-Zeldovich effect, and diffuse foregrounds in temperature and polarization.
- Catalogers of compact Galactic and extra-galactic sources (including separate catalogs of Sunyaev-Zeldovich clusters and Galactic cold clumps).
- Simulations of signals and noise used in assessing the performance of the analysis methods and assessment of uncertainties.
-

Planck 2015 : Data Products

February 2015

- Cleaned and calibrated timelines of the data for each detector at 30, 44, 70, 353, 545 and 857 GHz, and for the (unpolarized) spider-web bolometers at 100, 143, and 217 GHz.
- Maps of the sky at nine frequencies (Sect. 7) in temperature, and at 30, 44, 70, and 353 GHz in polarization. Additional products serve to quantify the characteristics of the maps to a level adequate for the science results being presented, such as noise maps, masks, and instrument characteristics.
- Four high-resolution maps of the CMB sky in temperature and polarization, and accompanying characterization products (Sect. 8.1).
- Four high-pass-filtered maps of the CMB sky in polarization, and accompanying characterization products (Sect. 8.1).
- A low-resolution CMB temperature map (Sect. 8.1) used in the low- ℓ likelihood code, with an associated set of foreground temperature maps produced in the process of separating the low-resolution CMB from foregrounds, with accompanying characterization products.
- Maps of thermal dust and residual cosmic infrared background (CIB), carbon monoxide (CO), synchrotron, free-free, and spinning dust temperature emission, plus maps of dust temperature and opacity (Sect. 9).

- Maps of synchrotron and dust polarized emission.
- A map of the estimated CMB lensing potential over 70 % of the sky.
- A map of the Sunyaev-Zeldovich effect Compton parameter.
- Monte Carlo chains used in determining cosmological parameters from the *Planck* data.
- The Second *Planck* Catalogue of Sunyaev-Zeldovich Sources (PSZ2, Sect. 9.2), comprising a list of sources detected by their SZ distortion of the CMB spectrum. The PSZ2 supersedes the previous Early Sunyaev-Zeldovich Catalogue ([Planck Collaboration XXIX 2014](#)) and the PSZ1 ([Planck Collaboration XXIX 2014](#)).
- The *Planck* catalogue of Galactic Cold Clumps (PGCC, [Planck Collaboration XXVIII 2015](#)), providing a list of Galactic cold sources over the whole sky (see Sect. 9.3). The PGCC supersedes the previous Early Cold Core Catalogue (ECC), part of the Early Release Compact Source Catalogue (ERCSC, [Planck Collaboration VII 2011](#)).

March 2015

- A likelihood code and data package used for testing cosmological models against the *Planck* data, including both the CMB (Sect. 8.4.1) and CMB lensing (Sect. 8.4.2).
- The Second *Planck* Catalogue of Compact Sources (PCCS2, Sect. 9.1), comprising lists of compact sources over the entire sky at the nine *Planck* frequencies. The PCCS2 includes polarization information, and supersedes the previous Early Release Compact Source Catalogue ([Planck Collaboration XIV 2011](#)) and the PCCS1 ([Planck Collaboration XXVIII 2014](#)).
- A full set of simulations, including Monte Carlo realizations.

Late spring/early summer 2015

- Cleaned and calibrated timelines of the data for all polarization-sensitive bolometers at 100, 143, and 217 GHz.
- Maps of the sky at 100, 143, and 217 GHz in polarization. Additional products serve to quantify the characteristics of the maps to a level adequate for the science results being presented, such as noise maps, masks, and instrument characteristics.

Component separation

The following four methods have been used for component separation/map making:

- SMICA
- NILC
- SEVAM
- COMMANDER

SMICA

- Principle:

SMICA produces a CMB map by linearly combining all Planck input channels (from 30 to 857 GHz) with weights which vary with the multipole. It includes multipoles up to $\ell = 4000$.

- Resolution (effective beam):

The SMICA map has an effective beam window function of 5 arc-minutes, deconvolved from the pixel window. It means that, ideally, one would have $C_\ell(\text{map}) = C_\ell(\text{sky}) * B_{(5')}^2$, where $C_\ell(\text{map})$ is the angular spectrum of the map, where $C_\ell(\text{sky})$ is the angular spectrum of the CMB and $B_{(5')}$ is a 5-arcminute Gaussian beam function.

- Confidence mask:

a confidence mask is provided which excludes some parts of the Galactic plane, some very bright areas and the masked point sources.

- Invalid pixels:

SMICA combines the input maps after some regions with strong emission have been replaced by a smooth fill-in (in order to mitigate spectral leakage). This is done over 3% of the sky, as indicated by the field INPMASK in the SMICA CMB FITS file. See the resulting obvious deficit of the CMB signal close to the Galactic plane in the above thumbnail.

NILC

NILC is a linear method for combining the input channels. It implements an ILC with weighting coefficients varying over the sky and over the multipole range up to $\ell = 3200$ and it does so using 'needlets' which are spherical wavelets. A special procedure is used for processing the coarsest needlet scale which contains the large scale multipoles.

SEVEM

The aim of Sevem is to produce clean CMB maps at one or several frequencies by using a procedure based on template fitting. The templates are internal, i.e., they are constructed from Planck data, avoiding the need for external data sets, which usually complicates the analyses and may introduce inconsistencies. The method has been successfully applied to Planck simulations Leach et al., 2008 and to WMAP polarisation data Fernandez-Cobos et al., 2012. In the cleaning process, no assumptions about the foregrounds or noise levels are needed, rendering the technique very robust.

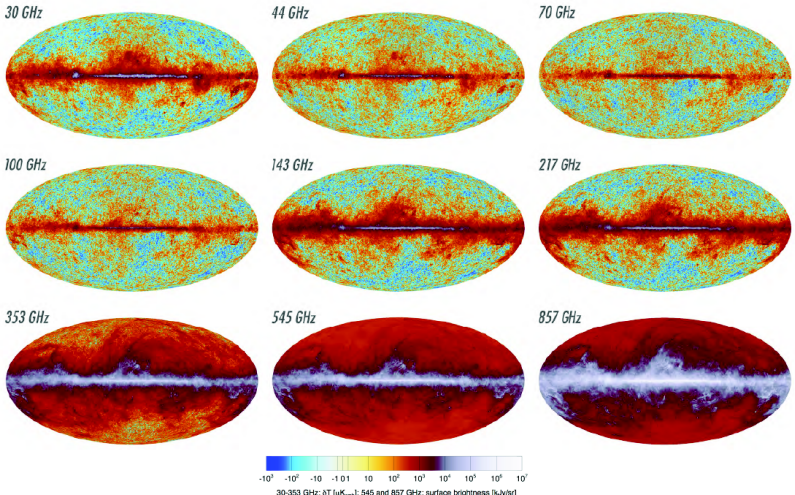
The input maps used are all the Planck frequency channels. In particular, we have cleaned the 100, 143 GHz and 217 GHz maps using four templates constructed as the difference of the following Planck channels (smoothed to a common resolution): (30-44) GHz, (44-70) GHz, (545-353) GHz and (857-545)GHz.

The templates are constructed by subtracting two neighbouring Planck frequency channel maps, after first smoothing them to a common resolution to ensure that the CMB signal is properly removed. A linear combination of the templates is then subtracted from the Planck sky map at the frequency to be cleaned, in order to produce the clean CMB. The coefficients of the linear combination are obtained by minimising the variance of the clean map outside a given mask. Although we exclude very contaminated regions during the minimization, the subtraction is performed for all pixels and, therefore, the cleaned maps cover the full-sky (although we expect that foreground residuals are present in the excluded areas).

Commander-Ruler

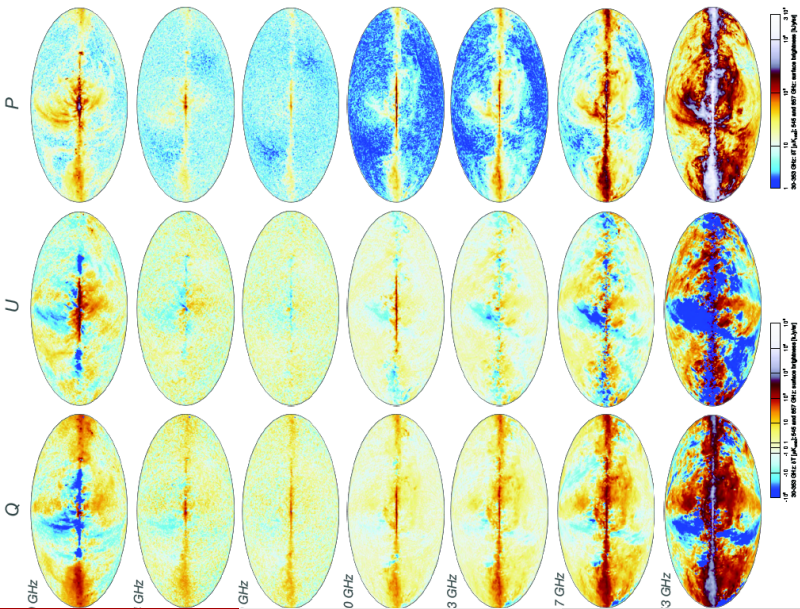
The Commander-Ruler (C-R) approach implements Bayesian component separation in pixel space, fitting a parametric model to the data by sampling the posterior distribution for the model parameters. For computational reasons, the fit is performed in a two-step procedure: First, both foreground amplitudes and spectral parameters are found at low-resolution using MCMC/Gibbs sampling algorithms (Jewell et al. 2004; Wandelt et al. 2004; Eriksen et al. 2004, 2007, 2008). Second, the amplitudes are recalculated at high resolution by solving the generalized least squares system (GLSS) per pixel with the spectral parameters fixed to their values from the low-resolution run.

For the CMB-oriented analysis presented in this paper, we only use the seven lowest Planck frequencies, i.e., from 30 to 353 GHz. We first downgrade each frequency map from its native angular resolution to a common resolution of 40 arcminutes and re-pixelize at HEALPix $N = 256$. Second, we set the monopoles and dipoles for each frequency band using a method that locally conserves spectral indices (Wehus et al. 2013, in preparation). We approximate the effective instrumental noise as white with an RMS per pixel given by the Planck scanning pattern and an amplitude calibrated by smoothing simulations of the instrumental noise including correlations to the same resolution. For the high-resolution analysis, the important pre-processing step is the upgrading of the effective low-resolution mixing matrices to full Planck resolution: this is done by repixelizing from $N = 256$ to 2048 in harmonic space, ensuring that potential pixelization effects from the low-resolution map do not introduce sharp boundaries in the high-resolution map.



Planck Collaboration: The *Planck* mission

Fig. 7. The nine *Planck* frequency maps show the broad frequency response of the individual channels. The color scale (identical to the one used in 2013), based on inversion of the function $y = 10^x - 10^{-x}$, is tailored to show the full dynamic range of the maps.



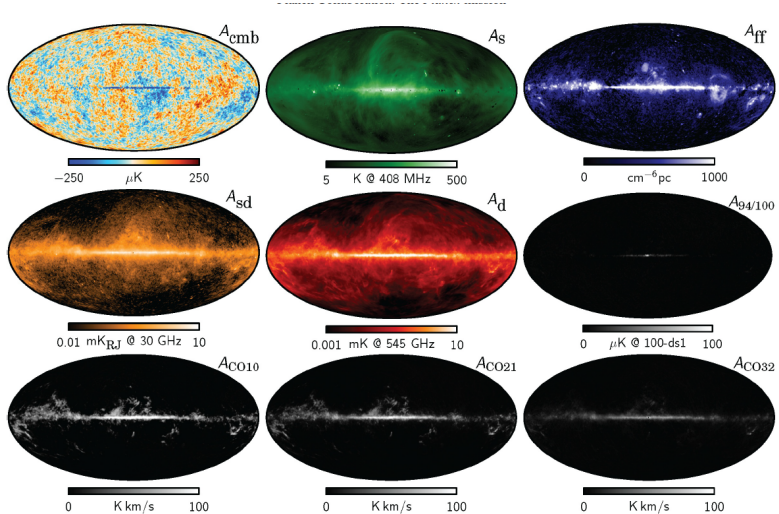


Fig. 14. Maximum posterior intensity maps derived from the joint analysis of *Planck*, WMAP, and 408 MHz observations (Planck Collaboration X 2015). From left to right, top to bottom: CMB; synchrotron; free-free; spinning dust; thermal dust; line emission around 90 GHz; CO $J = 1 \rightarrow 0$; CO $J = 2 \rightarrow 1$, and CO $J = 3 \rightarrow 2$.

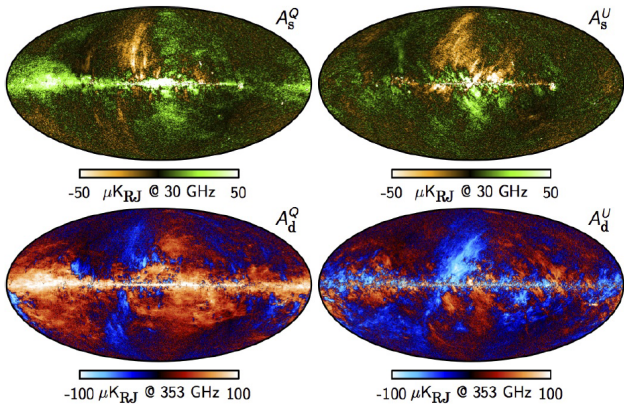
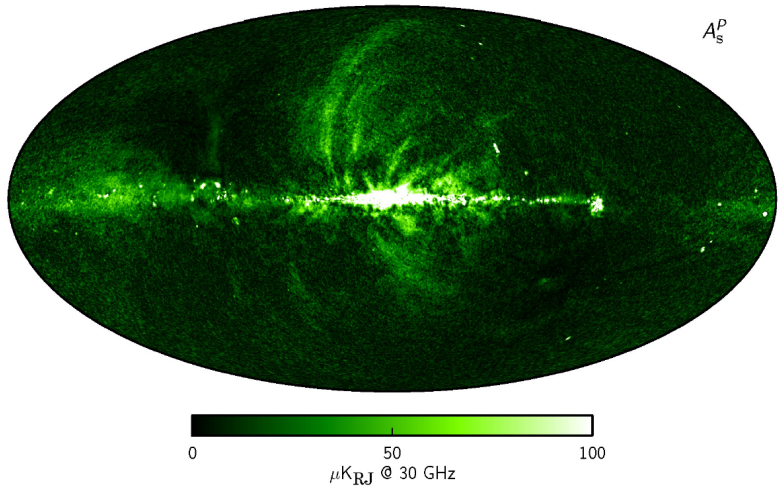
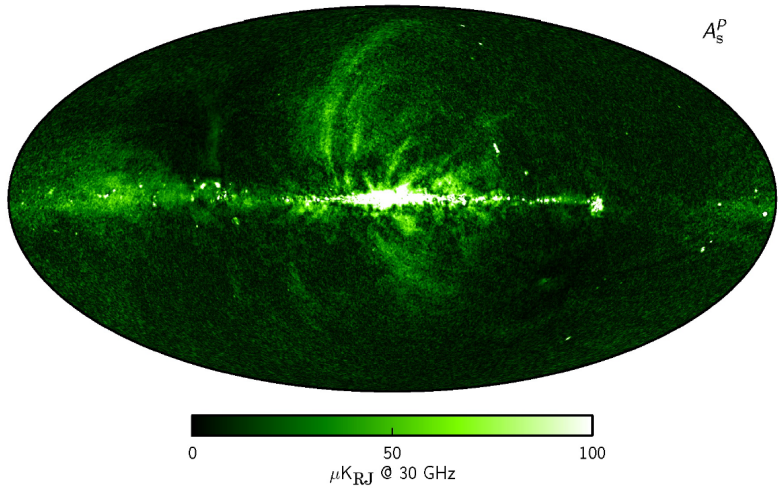


Fig. 15. Maximum posterior amplitude polarization maps derived from the *Planck* observations between 30 and 353 GHz (Planck Collaboration X 2015). The left and right columns show the Stokes Q and U parameters, respectively. Rows show, from top to bottom: CMB; synchrotron polarization at 30 GHz; and thermal dust polarization at 353 GHz. The CMB map has been highpass-filtered with a cosine-apodized filter between $\ell = 20$ and 40 , and the Galactic plane (defined by the 17 % CPM83 mask) has been replaced with a constrained Gaussian realization (Planck Collaboration IX 2015).





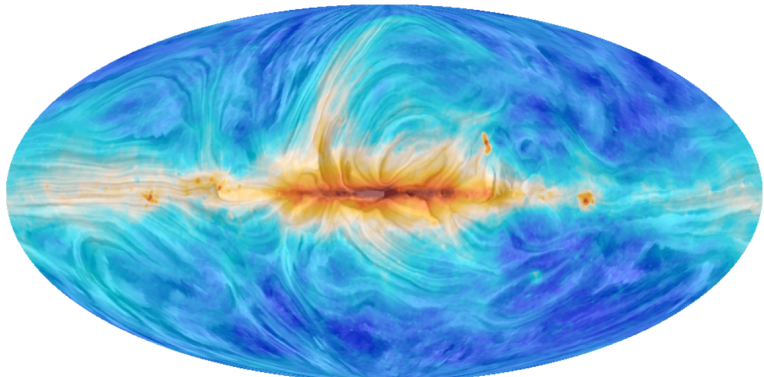


Fig. 20. All-sky view of the magnetic field and total intensity of synchrotron emission measured by *Planck*. The colours represent intensity. The “drapery” pattern, produced using the line integral convolution (LIC, [Cabral & Leedom 1993](#)), indicates the orientation of magnetic field projected on the plane of the sky, orthogonal to the observed polarization. Where the field varies significantly along the line of sight, the orientation pattern is irregular and difficult to interpret.

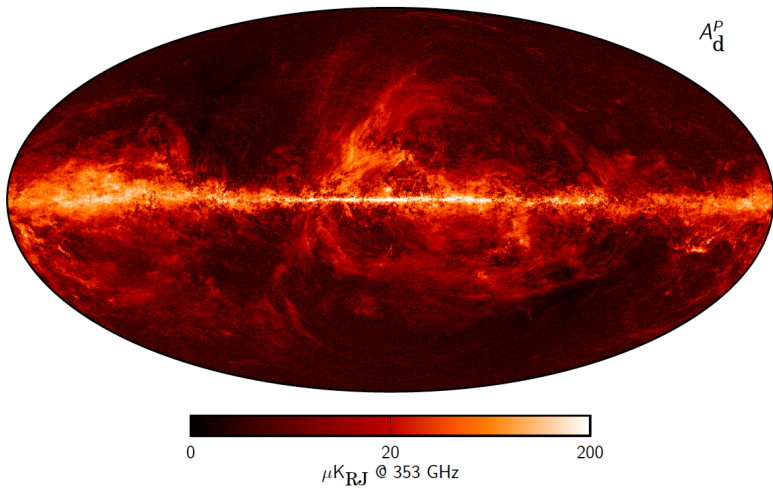


Fig. 21. Dust polarization amplitude map, $P = \sqrt{Q^2 + U^2}$, at 353 GHz, smoothed to an angular resolution of $10'$, produced by the diffuse component separation process described in ([Planck Collaboration X 2015](#)) using *Planck* and WMAP data.

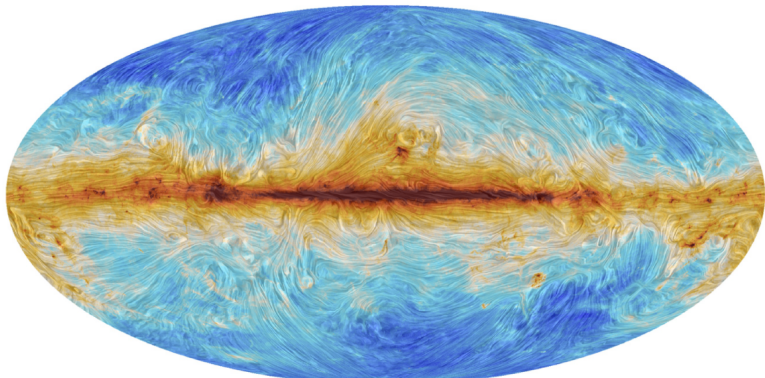


Fig. 22. All-sky view of the magnetic field and total intensity of dust emission measured by *Planck*. The colours represent intensity. The “drapery” pattern, produced using the line integral convolution (LIC, [Cabral & Leedom 1993](#)), indicates the orientation of magnetic field projected on the plane of the sky, orthogonal to the observed polarization. Where the field varies significantly along the line of sight, the orientation pattern is irregular and difficult to interpret.

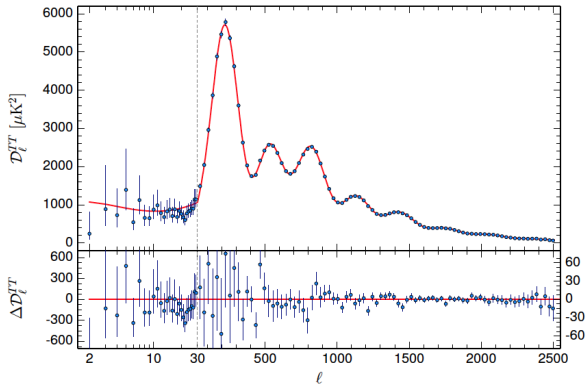


Fig. 9. The *Planck* 2015 temperature power spectrum. At multipoles $\ell \geq 30$ we show the maximum likelihood frequency averaged temperature spectrum computed from the Plik cross-half-mission likelihood with foreground and other nuisance parameters determined from the MCMC analysis of the base ΛCDM cosmology. In the multipole range $2 \leq \ell \leq 29$, we plot the power spectrum estimates from the Commander component-separation algorithm computed over 94 % of the sky. The best-fit base ΛCDM theoretical spectrum fitted to the *Planck* TT+lowP likelihood is plotted in the upper panel. Residuals with respect to this model are shown in the lower panel. The error bars show $\pm 1 \sigma$ uncertainties. From [Planck Collaboration XIII \(2015\)](#).

Temperature power spectrum

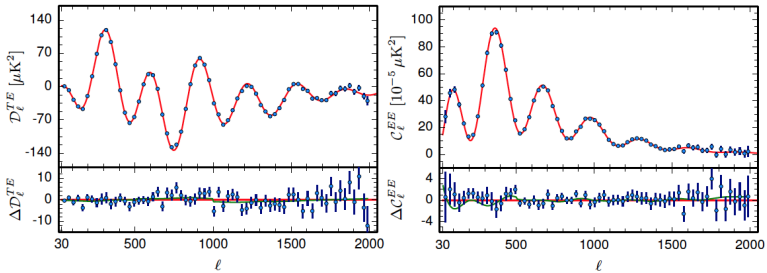


Fig. 10. Frequency-averaged TE (left) and EE (right) spectra (without fitting for $T-P$ leakage). The theoretical TE and EE spectra plotted in the upper panel of each plot are computed from the best-fit model of Fig. 9. Residuals with respect to this theoretical model are shown in the lower panel in each plot. The error bars show $\pm 1\sigma$ errors. The green lines in the lower panels show the best-fit temperature-to-polarization leakage model, fitted separately to the TE and EE spectra. From [Planck Collaboration XIII \(2015\)](#).

Polarization power spectra

Table 7. *Planck* peak positions and amplitudes.

| PEAK | | |
|--------------------------|---------------------|-------------------------------|
| Number | Position [ℓ] | Amplitude [μK^2] |
| <i>TT</i> power spectrum | | |
| First | 220.0 \pm 0.5 | 5717 \pm 35 |
| Second..... | 537.5 \pm 0.7 | 2582 \pm 11 |
| Third | 810.8 \pm 0.7 | 2523 \pm 10 |
| Fourth | 1120.9 \pm 1.0 | 1237 \pm 4 |
| Fifth | 1444.2 \pm 1.1 | 797.1 \pm 3.1 |
| Sixth | 1776 \pm 5 | 377.4 \pm 2.9 |
| Seventh | 2081 \pm 25 | 214 \pm 4 |
| Eighth | 2395 \pm 24 | 105 \pm 4 |
| <i>TE</i> power spectrum | | |
| First | 308.5 \pm 0.4 | 115.9 \pm 1.1 |
| Second..... | 595.3 \pm 0.7 | 28.6 \pm 1.1 |
| Third | 916.9 \pm 0.5 | 58.4 \pm 1.0 |
| Fourth | 1224 \pm 1.0 | 0.7 \pm 0.5 |
| Fifth | 1536 \pm 2.8 | 5.6 \pm 1.3 |
| Sixth | 1861 \pm 4 | 1.2 \pm 1.0 |
| <i>EE</i> power spectrum | | |
| First | 137 \pm 6 | 1.15 \pm 0.07 |
| Second..... | 397.2 \pm 0.5 | 22.04 \pm 0.14 |
| Third | 690.8 \pm 0.6 | 37.35 \pm 0.25 |
| Fourth | 992.1 \pm 1.3 | 41.8 \pm 0.5 |
| Fifth | 1296 \pm 4 | 31.6 \pm 1.0 |

Lensing Potential

5.1. CMB lensing measured by Planck

Gravitational lensing by large-scale structure leaves imprints on the CMB temperature and polarization that can be measured in high angular resolution, low noise observations, such as those from *Planck*. The most relevant effects are a smoothing of the acoustic peaks and troughs in the *TT*, *TE*, and *EE* power spectra, the conversion of *E*-mode polarization to *B*-mode, and the generation of significant non-Gaussianity in the form of a non-zero connected 4-point function (see [Lewis & Challinor 2006](#) for a review). The latter is proportional to the power spectrum $C_\ell^{\phi\phi}$ of the lensing potential ϕ , and so one can estimate this power spectrum from the CMB 4-point functions. In the 2013 *Planck* release, we reported a 10σ detection of the lensing effect in the *TT* power spectrum (see [PCP13](#)) and a 25σ measurement of the amplitude of $C_\ell^{\phi\phi}$ from the *TTTT* 4-point function ([Planck Collaboration XVII 2014](#)). The power of such lensing measurements is that they provide sensitivity to parameters that affect the late-time expansion, geometry, and matter clustering (e.g., spatial curvature and neutrino masses) *from the CMB alone*.

References

- ① Planck 2015 results. I. Overview of products and scientific results
[arXiv:1502.01582 [astro-ph.CO]]
- ② Planck 2015 results. XI. CMB power spectra, likelihoods, and robustness of parameters [arXiv:1507.02704 [astro-ph.CO]]
- ③ Planck 2015 results. XIII. Cosmological parameters [arXiv:1502.01589 [astro-ph.CO]]